International Journal of Civil, Structural, Environmental and Infrastructure Engineering Research and Development (IJCSEIERD)
ISSN(P): 2249-6866; ISSN(E): 2249-7978
Vol. 3, Issue 5, Dec 2013, 249-268

FAILURE MECHANISM FOR CONFINED PLAIN CONCRETE COLUMN

ATA EL-KAREIM S. SOLIMAN

Department of Civil Engineering, Faculty of Engineering Mataria, Helwan University, Egypt

ABSTRACT

In reinforced concrete structures, fiber reinforced polymer (FRP) confined concrete columns is one of the most attractive techniques used, but two problems delayed its wide spread. The first is the effect of column slenderness ratio, and column diameters and heights. The second problem is to accurately calculate the ultimate confined strength. Tested results of the eight polyvinylchloride tubes (PVC) confined concrete columns are used to study the behavior of confined columns. In addition, experimental results of eight plain concrete columns carried out for comparing between confined and unconfined column behavior. The theoretical prediction of confined compressive strength by using ultimate limit state method based on computability deformations is presented. In the paper, crack propagation and modes of failure were described. Analyses of the experimental results with the effect of column heights and diameters were discussed. The cracking behavior of confined concrete during loading is analyzed. The fracture compressive strain related to vertical stresses and corresponding axial strains, and fracture tensile strain related to horizontal acting stresses and corresponding radial strains are calculated. The experimental results showed that, the radial strains distribution may be not uniform through the hoop direction of confined columns.

KEYWORDS: Composite, Concrete, Confinement, Fracture Mechanics, Theoretical Model

BACKGROUND

The compression failure, and especially the size effect, is more complex and less understood. Yet it often the more important and dangerous mode of failure, which is highly brittle with less ductility, the reason is that compression failure is not controlled by material strength criterion, as assumed in nearly all practical applications up to now. When multi-axial experiments are carried out, the influence of boundary conditions in the experimental become extremely important. These influences are directly related to the deformability (both in the loading direction, as perpendicular to this direction) of the load-transmitting medium along the boundaries of specimen [1, 2].

Plastic pipes, tubing and profiles are used in a wide variety of industries including, building & construction, automotive, consumer goods, lawn & garden, windows & doors, furniture, plumbing and electrical. One of the most widely used materials for these products is polyvinylchloride or commonly known as PVC. This material is popular in these industries because of the wide range of properties that can be obtained depending on the additives that are mixed with it, all this at a relatively inexpensive price. The PVC is isotropic materials where the properties are the same in two directions. As in field of construction, when PVC plastic tube confined plain concrete column used instead reinforced concrete (RC) columns, the design equation is required. But, the all design equations for confined concrete columns are the empirical and related with experimental works [3, 5, 6, 7, 8, and 9]. The results of proposal equation were independent. Tables 1 shows the material properties used for experimental confinement compressive strength and strain, and table 2 shows some of equations used [8-14].

Silvia Rocca1 et al (2008) [15] reviews design guidelines for FRP confinement of reinforced concrete columns of

noncircular cross sections, and states that: approach presented by current ACI committee [16] for compressive strength is based on the empirical formula originally developed by Mander et al (1988) for steel confined concrete. Regarding CSA S806-02 guideline [17], the equation was obtained from experiments on cylindrical concrete confined under hydrostatic pressure [Richart et al. (1928)] and Saatcioglu and Razvi (1992) for confinement coefficient. The Concrete Society proposes a design-oriented model, developed by Lam and Teng (2003). And also, this model was calibrated against all the experimental data available at the time. The design recommendations provided by fib for columns of circular and noncircular cross sections are based on the model proposed by Spoelstra and Monti. From previous discussion, it can be concluded that the calculated confined compressive strength only depends on the experimental data. In this paper, the proposal theoretical model to calculate the ultimate confined compressive strength presents a new direction deserve important.

Three failures mechanics can be help for understand the confined failure mechanics are presented as the following: Hillerborg (1983) suggested that the actual flexural behavior of concrete could be attributed to the following four process zones. The first zone is elastic zone where linear elastic mechanics is applicable. The second zone is micro-cracking zone where the stiffness of the fracture zone decreases suddenly due to increasing micro-cracks. The third zone is micro-crack branching zone where multiple micro-cracks closed into one macro-crack and the stiffness of the fracture zone decreases slowly. Last zone is the traction free zone, where no stress transfer occurs across the fracture surface. The second is the failure mechanism of shear stress of reinforced concrete circular cross-section member. Finally the dowel action of steel bar through cracks caused stress concentration beside cracks. In the dowel action, it is found that the plastic hinge is situated 0.7-1.5d_p away from the shear plane and concentrated stress equal to 4.5 the cylinder compressive strength [18, 19, 20, 21].

In the reinforced concrete structures, using fiber reinforced plastic/polymer (FRP) with concrete and reinforced concrete is very wide spread. Only spread of FRP confined concrete and reinforced concrete columns is limited because of analytical models for calculating the confined compressive strength and lack of information about internal cracks in concrete core. The failure of confined concrete and the general proposal theoretical are the main problem. The main objective of this research describes the failure mechanics and calculates the ultimate confined strength of PVC-tube confined concrete.

THE EXPERIMENTAL WORK

In the experimental study, eight circular confined concrete (CC) columns were tested as listed in Table 3. For the first group, the column heights, H, were 300, 400, 600, 900mm and the cross sections were circular with 150.0 mm inner diameter and 4.7mm thickness. For the second group, the column heights, H, were 200, 300, 600, 900mm and the cross sections were circular with 110.0 mm inner diameter and 3.7mm thickness. The columns were tested until failure under the effect of axial load only. The materials used in preparing the test specimens were local available materials and the process of manufacturing was simulated as closely as to the common way of practices.

All specimens were cast in a vertical position on the same occasion and with concrete from the same batch. The used concrete was made from a mix of ordinary Portland cement, natural sand, and gravel. The average compressive strength of the unconfined concrete (UC) was 13.75MPa based on the compressive test result of standard cylinder (150x300mm). The experimental compressive strength of unconfined concrete with different heights is shown in Table 4. The mean value of concrete material properties at the age of 28 days were summarized in Table 5. For PVC tube, the average tensile strength of plastic tube was determined to be 53MPa and the elastic modulus was 35GPa.

A computerized universal-testing machine (U.T.M.) of 100-ton capacity was used to test the specimens as shown in figure 1-a. The load was incrementally applied to the column in specimen using compression state. Both the load (P_{exp}) and corresponding deflection (δ_{exp}) were recorded from the machine. From the area of loading (A_{load}) and the height of column (H) the stresses-strains curve was plotted.

The load was applied vertically at the center of the specimens. The load was applied to concrete section only. The radial strains were measured at 3 points on the outside of the plastic tube at mid-height of the columns, as shown in figure 1-b. The radial strains were measured and recorded using strain indicator connector which was connected to the strain gauges. Loading was applied using displacement control. Increments were increased by 0.2mm for each step with a rate of loading 25 kg/sec. There was a pause between each step to record the reading of strain gauges.

TEST RESULTS AND DISCUSSIONS

In this part, the mode of failures and observation cracks, stresses-strains (σ-ε) curves, and the effect of column slenderness ratio (λ) is summarized.

Test Observations and Modes of Failure

The interest of replacing conventional reinforced concrete columns by PVC tube confined concrete column causing of studied. The PVC tubes provide shear resistance, flexural resistance and confinement to the concrete core.

In the case of unconfined concrete columns, and for slenderness ratios 1.85, 2, 2.67, and 2.75 (for samples SUC6-30, SUC6-40, SUC5-20 and SUC5-30), the failures were generally marked by the appearance of vertical cracks at about 90% of the ultimate load followed by crushing of concrete at/or near the mid-height of the specimens as shown for specimen SUC6-40 in figure 2-a. There was no indication of any buckling until the concrete was completely crushed. But, for slenderness ratios 4.00, 5.78, 6.00, and 8.20 (samples SUC6-60, SUC6-90, SUC5-60 and SUC5-90), the failures were generally marked by the appearance of vertical cracks at about 65% of the ultimate load followed by longitudinal cracks in concrete lead to failure. The failure pattern were shown in figure 2-b. From this concluded that the longitudinal cracks begin of appearing for unconfined concrete column after 65% from the maximum load depending on the specimen's slenderness ratio.

In the case of confined column, in general, the observed behavior of the confined columns was similar to the unconfined columns up to the peak load of unconfined columns. Increases in the lateral deflection of confined columns resulted increased compression stresses and rupturing of the plastic tube. Tensile rupture of the tube was only caused by a significant increase in the lateral buckling beyond the peak load. The signs of distress to the composite were the heard sounds and the large lateral deflections of the columns. The failures of confined specimens SCC6-30, SCC6-40, SCC5-20 and SCC5-30) were generally marked by sudden fracture of the plastic tube near the top and bottom edges of the tube. The pattern failure for specimen SCC5-30 was shown in the figure 2-c. Sounds heard during the early to middle stages of loading were attributed to the micro-cracking of concrete and shifting of aggregates. After the peak load, the not equally uniform strain distributed through plastic tube. And snapping of the plastic tube could be heard near the end of the loading process. The failure of confined specimens SCC6-60, SCC6-90, SCC5-60 and SCC5-90 was generally due to shear cracks followed by yield of plastic tube. The crack patterns for confined concrete column specimen SCC5-60 was shown in figure.2-d. From this concluded that the composite materials confined concrete column not prevents cracks but the confinement restrains the development of cracks and delays formation a new crack. Moreover, the failure mechanisms change s by varying the slenderness ratios of tested specimens

Stress Strain (σ -ε) Curves

The stress strain curves (radial and axial strains) for group no.1 and no.2, for confined specimens, were shown in figures 3, and 4 respectively. There are three reading for radial strains ($\varepsilon_{cc,r}$) and one reading for axial strains ($\varepsilon_{cc,l}=\delta_{exp}/H$). The figures show that the relation between vertical stresses and radial strains not fixed especially according to place of reading. The stress-strain curves of concrete column confined by plastic tube are divided into two parts with changed slope. The first portion is essentially identical to that of the unconfined concrete. It is from the initial of loading up to the maximum load. In this part, the concrete gradually will be full active contact with PVC tube. For the radial strains, it was found that before 70% of the unconfined concrete stress, the three redial strains are identical, but, after 70% radial strains begin deviations. This appears especially for specimens SCC5-20, SCC5-30, SCC6-30, SCC6-40 and SCC6-60. The deviations of radial strains refer to formation internal cracks in the concrete core. And deviations of radial strains (three curves for one specimen) were related to the positioning of gauges relative the cracks.

In the second part of curves, the radial and axial strains increased with decreasing in loads. This means that the concrete is expanding rapidly with a small changing in stresses, causing a large increase in lateral expansion. The curves are agreement with previous studied [10].

From this concluded that, the most deviation of radial strains values (three curves for one specimen) credits to the positioning of gauges relative the cracks that begin initiated.

Effect of the Column Dimensions on the Ultimate Stresses and Strains

In this study and through previous research, it has been proven that used FRP confined concrete columns provides superior ductility and improves the load carrying capacity characteristics when comparing to conventional columns. The effect of columns dimensions is discussed in table 6 and figure 6.

For group 1, with 150mm diameters, the ratios between the confined concrete strength (f_{cc}) and characteristic concrete compressive strength at 28 day (f_{co}) are from 2.22 to 2.39, and for group 2, with diameters 110mm, are from 2.60 to 4.30. From these ratios find that by decreasing the column diameters, the efficiency of confined enhanced. From figure 6 find that, for slenderness ratio more three, the effect of diameters in the same slenderness ratio on the radial and axial strain is not significant as ultimate confined strength. But for slenderness ratio less than 3, the effect of diameters with the same slenderness ratio is not clear. From tables 6 and figure 6 concluded that, with slenderness ratio more or equal than three the tested specimens defined as columns. In contrary, for with slenderness ratio less than three the tested specimens defined as cylinder.

In the other direction, as shown in figure 6, for group 1, with 150mm diameters, the ratio between confined concrete strength with different heights (f_{cc}) to the confined concrete strength with column height equal to 900mm ($f_{cc,h}$) is analysis. And the ratios $f_{cc}/f_{cc,h}$ for heights H=900, 600, 400, and 300mm are 1, 1.07, 1.33, and 1.35 respectively. For group 2, with 110mm diameters, the ratios $f_{cc}/f_{cc,h}$ for heights H=900, 600, 300, and 200mm are 1, 1.01, 1.18, and 1.35 respectively. Moreover, for group 1, with 150mm diameters, the ratio between confined concrete strength with different heights (f_{co}) to the ratio of confined concrete strength with column height equal to 900mm ($f_{co,h}$) is analysis. And the ratios f_{co} / $f_{co,h}$ for heights H=900, 600, 400, and 300mm are 1, 1.28, 1.33, and 1.51 respectively. For group 2, with 110mm diameters, the ratio $f_{co}/f_{co,h}$ for heights H=900, 600, 300, and 200mm is 1, 1.06, 1.32, and 1.53 respectively. From this concluded the ratios of $f_{cc}/f_{cc,h}$ and $f_{co}/f_{co,h}$ refer to enhancement confined capacity by increasing the slenderness ratio.

THEORETICAL STUDY

In this part, the stages of change compatibility deformation between concrete core and FRP confined during loading are presented. Failure mechanism of confined concrete columns is illustrated. Moreover, the paper presents the proposal theoretical equation calculates the ultimate confined concrete strength. Finally, for completing nonlinear model, compression fracture strain energy per unite volume and tensile strain energy per unite volume is presented.

Stages of Change Compatibility between Concrete Core and Confined FRP

During loading, there are four stages having different behavior according to the boundary condition between the FRP sheet/tube and surface concrete core. The initial stage (the confinement action not fully acting); the elastic stage (the relation between stress and strain according to hook's low can be applied); the plastic-fracture stage (after cracking); the failure stage (after the peak load).

In the initial Stage, the quality of executing of the FRP around the concrete core influences the confinement action. In the presence of local misalignment fibers, a part of the circumferential deformation may be used to stretch the fibers. In this case, the concrete will not fully act with the FRP-tube [22, 23].

In the elastic stage, the tensile stress of FRP in the hoop direction and the contact stresses between FRP tube/sheet and concrete core are uniform. From compatibility deformation between the confined concrete core and FRP tube/sheet, the strain at the contact surface of concrete (ε_c) is equal to the FRP strain (ε_f). The linear hook's low cab be used in this stage. The stresses (f_{cc}) and strains (ε_{cc}) for confined concrete columns, in longitudinal direction, are calculated as the follows [22]:

$$f_{cc} = \frac{f_l}{\nu_c}[k] \tag{1}$$

$$\varepsilon_{cc} = -\frac{f_{cc}}{E_c}[1-\frac{2\nu_c^2}{k}] \tag{2}$$

Where $\frac{1}{k} = \frac{E_{\text{FRP}} t_f}{(1-\nu_c)E_{\text{FRP}} t_f + E_c r_t}$, t_f is the fiber thickness, r_t is the half concrete core diameter, and υ_c is the concrete poisson's ratio.

In the third stage, the cracks begin propagated. The confined concrete core cracks when the radial/or tangential strains in concrete more than the allowable concrete tensile strain ($\varepsilon \geq \varepsilon_{ct}$). The proposal theoretical model depends on the confined behavior in this stage.

Failure Mechanism and Deformability

FRP confined concrete structures are made up of two materials with different characteristics, namely, FRP tube/sheet and concrete. Bazant and Xiang (1997) illustrated the compression failure of unconfined concrete column. The crack model for confined concrete column, for macro scale, is shown in Figures 7. The crack band model was widely used in practice for analyzing the distributed cracking and fracture of the concrete [23, 24, and 25], and also, used for confined concrete failure. The concrete core is divided into number of units/segments and cracks equal to number n, and widths equal to b(r) as shown in Figure 7-a. the cracks appear when the tangent/or radial strain is more than the allowable tensile strain of the concrete. The real behavior of cracks, in the experimental tested specimens and by Cole, C. and

Belarbi, A (2001) as shown in figure 7-b [26], agrees with the assumption crack patterns. The radial cracks propagate, and the FRP tube/sheet restrains internal cracks in the concrete core

In the tangential direction, at the end of cracks, through contact surface between inner perimeter of FRP and the out perimeter of concrete core, the stresses in the FRP sheet/shell are not uniform. Two zones are as the follows:

The first zone lies between point (m_{2i-2}) and point (m_{2i-1}), where i is the number of cracks as shown in figure 7-a). The tangential/radial strains at perimeter of concrete core are less than allowable tensile strain. Thus, the crack width is equal to

$$w_{(r)} = b_{(r)}\varepsilon_o \tag{3}$$

Where ε_o is the tensile tangential/ radial strain

The second zone is between point (m_{2i-1}) and point (m_{2i}) (see figure 7-a). The tensile strain is more than the allowable tensile strain of concrete and less than the allowable tensile strain of FRP sheet/tube. Thus, cracks appearance in concrete core, and the crack width through widths equal to b(r) can be calculated as follows

$$w_{(r)} = b_{(r)}\varepsilon_o + w_{c_{(r)}} \tag{4}$$

Where $w_{c_{(r)}}$ is the crack width

The figure 8 shows the confined model in meso/or micro scale. At the contact surface between the concrete core and FRP sheet/tube, because of the allowable tensile strain between for FRP sheet and concrete is not equal, the differential movement happens. Subsequently two applying stresses occur, the first is a friction stress between the FRP sheet/tube and concrete core, and the second is the tensile strain of concrete core near the contact surface. At the same zone, the contact stress in the radial direction cause the third stress, as contact pressure (f_l) in the linear model [22]. From this concluded that the applied concentrated stress near crack tips could be created. The concentration stresses causes additional acting stresses to the applied vertical stress. More studied to understand the behavior of this zone in the meso/ or micro scale required.

Proposal Theoretical Model

In the present studied, beside the general assumption of fracture mechanics and presented failure mechanism of confined concrete column, the additional assumption of confined concrete can be as the follows:

- When the radial strain in the FRP tube is greater than the maximum allowable tensile strain of concrete, internal cracks propagate in the concrete core.
- The confinement concrete columns delay formation a new cracks, and not prevent it.
- The confinement of concrete column restrains development cracks.
- The FRP tube/sheet restrains deformation with a force called resistance force of FRP sheet/tube (R_{frp}). In addition, the tensile stress in the uncracked part is helping in the restraining with a force called resistance force of concrete (R_{ct}), the forces place is shown in figure 8-a.
- The horizontal applying tensile stress due to vertical stress causes tensile deformation of FRP tube/sheet with a force called acting force (C_{ver}), as shown in figure 8,

- Concentrated stresses besides the crack tips between point's m_{2i-1} and m_{2i} formed, and caused a force called acting force due to concentration stresses (C_{con}), as shown in figure 8-b.
- From equilibrium forces as shown in figure 8, the resistance forces (F_R) are equals to the acting forces (F_A.) .

$$\sum F_{R.} = \sum F_Z \tag{5}$$

Resistance Forces

Due to FRP tensile strength and concrete tensile strength, the resistance forces happen. The total resistance force, as shown in figure 8, can be calculated as follows:

$$\sum F_R = R_{frp} + R_{ct} \tag{6}$$

Assuming the resistance strength under the area (dA) is σ , the force (F) can be calculated as the follows:

$$F = \int \sigma \times dA \tag{7}$$

Where the area of stress has width b and length equal unity.

- The resistance force due to tensile strength of FRP sheet/tube is given by

$$R_{frp} = b\int_0^{t_{frp}} f_{frp}dy \quad = \varphi \times f_{frp} \times t_{frp} \tag{8}$$

Where φ is a factor accounting for the un-uniform strain distribution through the tangential direction and can be assumed equal to 0.8. Thus,

$$R_{frp} = 0.8 \times f_{frp} \times t_{frp} \tag{9}$$

- The resistance force due to tensile strength of concrete core is given by

$$R_{ct} = b\int_0^{r^*} f_t dr \tag{10}$$

Where $r^* = r \times \dfrac{\varepsilon_{ct}}{\varepsilon_{frp}} + 0.5 \times l_p$, l_p is the fracture length depending on the material properties, ε_{ct} is the maximum allowable tensile strain, and ε_{frp} is the allowable tensile strain of fiber in the hoop direction.

Assuming the area of tensile stress is equal to a triangle with length equal to $r \times \varepsilon_{ct} / \varepsilon_{frp}$, and height equal to maximum tensile stress f_{tc}, thus

$$R_{ct} = \frac{1}{2} \times \left[(r \times E_{frp}) \Big/ \left(E_c \times f_{frp}\right) \right] \times f_{tc}^2 \ . \tag{11}$$

Acting Forces

The acting forces as a result of indirect horizontal stresses from applying vertical load and concentration stresses

at the end of crack near the contact surface between FRP sheet/tube and concrete core, as shown in figure 8, can be calculated as follows:

$$\sum F_A = C_{ver} + C_{con} \tag{12}$$

- The acting force due to vertical stress is given by

$$C_{ver} = b\int_0^{t_{frp}} f_{sp}dr \tag{13}$$

Where f_{sp} is a splitting tensile strength, and can be assumed as a function of the confined stress

$$f_{sp} = \mu_1 \times f_{cc} \tag{14}$$

Where μ_1 is the ratio between vertical force and the horizontal force, thus

$$C_{ver} = (\mu_1 f_{cc}) \times r \tag{15}$$

By using a strut-and-tie model, as in the case of post-tensioned and pre-stressed concrete structural members, and as illustrated by Ata El-kareim, the splitting force is calculated as follows [19, 22];

$$f_{sp} = 0.25 \times f_{cc} \times \left(\frac{t_{frp} \times E_{frp}}{r \times E_c + t_{frp} \times E_{frp}} \right) \tag{16}$$

From equation 15 and 16 find that

$$\mu_1 = 0.25 \times \left(\frac{t_{frp} \times E_{frp}}{rE_c + t_{frp} \times E_{frp}} \right) \tag{17}$$

Form equation 12 and 16, the force C_{ver} is equal to

$$C_{ver} = 0.25 \times \left(\frac{t_{frp} \times E_{frp}}{r \times E_c + t_{frp} \times E_{frp}} \right) \times f_{cc} \times r \tag{18}$$

- 0BActing force due to concentration stress calculates as the following:

1BThe acting force, as shown in figure 8, created at the zone between point m_{2i-1} and point m_{2i} due to concentration stress. Considering the average stress is equal to $(\mu_2 f_{cc})$ with length equal to $[(\xi \times t_{frp})]$, the force C_{con} can be as follows forms:

$$C_{con} = (\mu_2 f_{cc}) \times (\xi \times t_{frp}) \tag{19}$$

2BWhere μ_2 is the ratio between the maximum actual stresses to the confined vertical stress (f_{cc}). Assuming ratio $\mu_2 \times \xi$ is 3 equal to [20, 21]. Then, the force can be calculated as the follows.

$$C_{con} = 3 \times t_{frp} \times f_{cc} \tag{20}$$

Compensation on equation 5 by the equation 8, 11, 18, 20 find that

$$0.8\times f_{frp}\times t_{frp}+\frac{1}{2}\times\left[\frac{r\times E_{frp}}{E_c\times f_{frp}}\right]\times f_{tc}^2=0.25\times\left(\frac{t_{frp}\times E_{frp}}{r\times E_c+t_{frp}\times E_{frp}}\right)\times f_{cc}\times r+3\times t_{frp}\times f_{cc} \quad (21)$$

Thus, $$f_{cc}=\left[\frac{0.8\times f_{frp}\times t_{frp}+\frac{1}{2}\times\left[\frac{r\times E_{frp}}{E_c\times f_{frp}}\right]\times f_{tc}^2}{0.25\times\left(\frac{t_{frp}\times E_{frp}}{r\times E_c+t_{frp}\times E_{frp}}\right)\times r+3\times t_{frp}}\right] \quad (22)$$

By evaluating the equation 22 using the results of Nanni and Bradford, Harmon and et al, Picher and et. al., watanabe and et. al., Miyauchi and et. al., Kono and et al., Toutanji and et. al., Matthys and et. al., Shahawy and et. al. 2000, Rochette and Labossiere, Micelli and et. al., and Rousakis find that the ratios between the experimental confined strength ($f_{cc,exp}$) to theoretical confined strength calculated by equation 22 ($f_{cc,thoer}$) were not unity.

Figure 9 shows the relation between the ratios $f_{cc,ex}/f_{cc,the}$ and fiber thickness, unconfined concrete strength, ultimate tesile strength of FRP, and ultimate tensile strain of FRP. From figure 9 concluded that, by increasing the fiber thickness and decreasing the ultimate tensile strength of FRP sheet/tube, the ratios $f_{cc,ex}/f_{cc,the}$ come close to unity. And also, by increasing the concrete compressive strength and decreasing the ultimate strain of fiber the proposal equation efficiency may be enhancement [19].

4B3.4. Fracture Energy of Confined Concrete Columns

The addition of confinement around reinforced concrete cross sections changes the concrete's stress-strain behavior from relatively weak and brittle to strong and ductile. The added strength and ductility found in confined concrete is due to the development of a triaxial stress field and the containment of the concrete after cracking. Mander and et al. used an energy balance approach along with effectiveness coefficients to unify the confinement model for both circular and rectangular transverse reinforcement at various spacing. Mander's model was based on the equation suggested by Popovics in 1973 and has gained wide acceptance in the Civil Engineering [14].

In the proposal model, two fracture strain energy per unite volume calculate; the first is compression strain energy per unite volume (G_c), and the second is the tensile strain energy per unite volume (G_f). The compression strain energy per unite volume (G_c) can be equal to the area under curve (f_{cc}-ε_{axial}), where f_{cc} is the vertical confined compression stress, and ε_{axial} is the corresponding axial strain. The tensile strain energy per unite volume (G_f) can be equal to the area under curve ($\sigma_{act.horz}$-ε_{radial}). Where $\sigma_{act.horz}$ is the acting horizontal stress, and ε_{radial} is the corresponding tangent/radial strain. In the present paper, the acting horizontal stress.

5B4. COMPARISON BETWEEN EXPERIMENTAL RESULTS AND THEORTICAL EQUATIONS

In this part, for PVC tubes confined concrete, the proposal theoretical equation calculates the confined compressive strength presented. Comparing among the proposal theoretical equation before and after calibration, different proposal analytical models, and experimental results is done. Finally, the values of compressive strain energy (G_c) per unit volume and tensile strain (G_f) per unit volume is presented.

6BProposal Design Equation for Confined Concrete Columns

In general, the proposal theoretical confined concrete strength can be as the following:

$$f_{cc,\exp}=f_{cc,theor}\times k_1\times f(\lambda) \quad (23)$$

Where k_1 is experimental factor, and can be assumed to calculate as the ratio between experimental confined strength to theoretical confined strength when column slenderness ratio is equal to 3 [$k_1 = f_{cc,\exp} / f_{cc,theor} \big|\ \ for\ \ \lambda = h/d = 3$]. And $f(\lambda)$ is experimental factor, takes the effect of column slenderness ratio into considerations.

Thus, the experimental factor (k_1), for specimens with slenderness ratio near from 3, as shown in table 6, can be approximate to 2.25. Moreover ,using excel programs and having best fitting, as shown in figure 10, the factor $f(\lambda)$ can be approximate to $\frac{4.0}{\lambda^{0.88}}$.

Then, the final proposal equation for PVC tube confined concrete tested specimens is as follows:

$$f_{cc} = \begin{cases} \left[\dfrac{0.8 \times f_{frp} \times t_{frp} + \frac{1}{2} \times \left[\dfrac{r \times E_{frp}}{E_c \times f_{frp}} \right] \times f_{tc}^2}{0.25 \times \left(\dfrac{t_{frp} \times E_{frp}}{r \times E_c + t_{frp} \times E_{frp}} \right) \times r + 3 \times t_{frp}} \right] \times 2.25 & for \lambda \le 3 \\ \left[\dfrac{0.8 \times f_{frp} \times t_{frp} + \frac{1}{2} \times \left[\dfrac{r \times E_{frp}}{E_c \times f_{frp}} \right] \times f_{tc}^2}{0.25 \times \left(\dfrac{t_{frp} \times E_{frp}}{r \times E_c + t_{frp} \times E_{frp}} \right) \times r + 3 \times t_{frp}} \right] \times 2.25 \times \dfrac{4.0}{\lambda^{0.88}} & for\ \lambda \succ 3 \end{cases} \tag{24}$$

Strain Energy of Confined Concrete Model

By using figures 3, and 4, the compression strain energy per unit volume defined as the area under f_{cc}-ε_{axial} curve, where f_{cc} is vertical applying stress and ε_{axial} is corresponding axial strain. And also, the tensile strain energy per unit volume (G_f) defined as the area under $\sigma_{act.horz.}$-ε_{radial} curve, where $\sigma_{act.horz}$ is the acting horizontal stress and ε_{radial} is the corresponding radial strain. Where the acting horizontal stress is approximately equal to the splitting tensile stress calculate by equation no. 16. Figure 11 shows the relation between the calculated acting horizontal stresses and corresponding radial strains for group no. 1 and no. 2.

Table 7 presents the compression strain energy per unit volume [G_c MPa/(mm/mm)], the tensile strain energy per unit volume [G_f MPa/(mm/mm)], and the ratio between G_c /$G_{f.}$. The compression strain energy of confined specimens SCC6-30, SCC6-40, SCC6-60 and SCC6-90 were 0.424, 0.2195, 0.0969 and 0.0551 MPa/(mm/mm) respectively. And also compression strain energy of confined specimens SCC5-20, SCC5-30, SCC5-60 and SCC5-90 where 0.354, 0.1918, 0.0907, and 0.079 MPa/(mm/mm). The tensile strain energy of confined specimens SCC6-30, SCC6-40, SCC6-60 and SCC6-90 were 0.0187, 0.00856, 0.00466 and 0.00578MPa/(mm/mm) respectively. And also tensile strain energy of confined specimens SCC5-20, SCC5-30, SCC5-60 and SCC5-90 where 0.0067, 0.00539, 0.00361, and 0.0056MPa/(mm/mm). As shown in figure 12, by drawing the relation between the compression and tensile strain energies and slenderness ratios concluded that by increasing the slenderness ratio, the compression and tensile strain energy per unit volume decreased. Furthermore, the strain energy depends on the specimen's size

7B4.3. Comparing Between Experimental Results and Different Theoretical Results

As in the field of construction, when PVC plastic tube confined plain concrete column used instead R.C. columns, the design equation is required. But, the reviewing design equations depend on the empirical equation calibrated by experimental results not totally included the same materials properties. Table 8 shows comparing between the experimental results of equation 22 and final equation (25), several analytical models as the following.

For saadatm et. al. model, for the short confined concrete columns, the ratio between experimental and theoretical values is from 0.71 to 1.19 but for long confined concrete columns the ratios are from 0.18 to 0.22. And this results agree with saamen et. al. and Toutanji equations results also. From this concluded that the equations not take the effect of column slenderness ratio into considerations. By using kono et al. and Miyauchie et al. models find that the equations for confined compressive strength is conservative for short confined concrete column, where the ratios between experimental to theoretical is more than 1.36, and also not take the effect of column slenderness ratios into considerations. Moreover, the theoretical confined compressive strength by Kono et al equation is 14.42 N/mm^2, and 14.62 N/mm^2 and the theoretical results by equations No. 22 (the proposal theoretical results without verification) are 12.19N/mm^2 and 12.43 N/mm^2. Form this concluded that the results of proposal theoretical equation (eq.22) can be consider as the results of analytical proposal equation by Kono and et. al.

By using equations 25, the ratios between experimental and theoretical are from 0.81 to 1.15 regardless the tested specimens SCC5-90 result.

8B5. FUTURE RECOMMENDED STUDIED

More experimental and theoretical studies are required for this model to calculate the characteristic fracture process zone length l_p^* , the local concentrated stress around crack tips with factors μ, ξ, compression strain energy (G_c) per unite volume, and tensile strain energy be unit volume (G_f).

CONCLUSIONS

From theoretical studied of mechanism of failure of FRP tube confinement concrete the following conclusions can be drawn:

- The mode of failure changes by altering slenderness ratio of the confinement concrete column.
- FRP tube/sheet confinement concrete makes a restrain for crack and delays the crack development but not prevents internal cracks.
- The ultimate confined compression strength can be theoretically calculated by equation 22. with experimental calibration
- The maximum confined compression strength depends not only on material properties ($E_{frp}, f_{frp}, E_c, f_{ct}$), but also on the size of specimen effect [h, r, t_{frp}].

REFERENCES

1. Bazant Z.P. and Xiang. Y., (1997) “Size effect in compression fracture: splitting crack band propagation,” journal of engineering mechanics, feb. pp. 162 – 172.

2. Bazant Z.P., and et al. (1993) “Fracture energy release and size effect in borehole breakout,” International journal numerical and analytical methods in geomech. No. 17, pp.1 – 14.

3. Ata El-kareim Shoeib, (2009)“Theoretical study of effect of slenderness ratio on the concrete filled FRP tube”. Technology of building material journal, Russia. No.1, pp. 4 -5.

4. Ata El-kareim Shoeib (2011) "Behavior of long confined concrete column” Sci. Bull. Fac. Eng. Ain Shams Univ. Egypt – received March, 2011, Elsevier Science Ltd., London, UK.

5. Fouad, Khairallah, and Ata El-kareim Shoeib (2006) "Experimental analysis of filled tube long concrete columns” Sci. Bull. Fac. Eng. Ain Shams Univ. Egypt – vol.41. No. 4, P185 – 199.

6. Khairallah, Fouad and Ata El-kareim Shoeib (2009) “Theoretical analysis of confinement short concrete column” Conference of Industry of Engineering Construction Between Reality & Ambitions, Al Baath University, Syria - Vol. 1 – pp. 141 – 156.

7. Hamdy M. and Radhouane M. (2010) “Axial Load Capacity of Concrete-Filled FRP Tube Columns: Experimental versus Theoretical Predictions” Journal of composites for construction. pp. 231 – 243.

8. Kono S. and et al. (1998) “Evaluation of confining effects of CFRP sheets on reinforced concrete members”. Proceedings of the 2nd international conferences on composites in infrastructure ICCI 98, Tueson, Arizona. pp. 343 – 355.

9. Miyauchi K. and et al. (1997) “Estimation of strengthening effects with carbon fiber sheet for concrete column”. Proceedings of the third international symposium (FRPRCS-3) on Non-Metallic (FRP) Reinforcement for concrete structures, Sapporo, Japan, pp. 217 – 224.

10. Toutanji, H. A. (1999) “Stress – strain characteristics of concrete columns externally confined with advanced fiber composite sheet” ACI structural journal, V. 96, No. 3, pp. 397-405.

11. Samaan M, and et al. (1998) “Model of concrete confined by fiber composites”. Journal of Structure Engineering, ASCE, V. 124, No.9, pp 1025 –1031.

12. Saafi H., and Toutanji, Z. Li (1999) “Behavior of concrete columns confined with fiber reinforced polymer tubes,” ACI material journal, V. 96, No. 4, pp. 500 – 509.

13. Y. Xiao and H. Wu, P., (2000) “Compressive behavior of concrete confined by carbon fiber composite jackets". J Mater Civ. Eng. ASCE, V. 2, No. 12, pp. 139 - 146.

14. Mander, J. B., Priestley J.N., and Rark R., (1988) “Theoretical Stress-Strain Model for Confined Concrete,” Journal of Structural Engineering, ASCE. V. 144, No. 8, pp. 1804 – 1826.

15. Silvia Rocca1 et al (2008) “Review of design guidelines for FRP confinement of reinforced concrete columns of noncircular cross sections.” Journal of composites for construction. Jan/Feb. pp. 80 – 92.

16. American Concrete Institute ACI. (2002). “Guide for the design and construction of externally bonded FRP systems for strengthening of concrete structures.” ACI 440.2R-02, Farmington Hills, Mich.

17. Canadian Standards Association CSA. (2002) “Design and construction of building components with fiber-reinforced polymers.” CSA-S806, Rexdale, Ont., Canada.

18. Hillerborg A. (1983), “Analysis of one single crack” Fracture Mechanics of Concrete, Elsevier Science Publisher, Amsterdam, P. 223-249.
19. Ata El-kareim Shoeib (2011) "Concepts and mechanisms of failure in FRP confinement concrete column-part II” Faculty of Engineering Mataria journal, Helwan Univ, Egypt.
20. Ata El-kareim Shoeib (2001) “Punching shear resistance of reinforced concrete flat slab" Master, thesis, Faculty of engineering, Helwan university Egypt, P. 207.
21. Frenay (1990) “Theory and experiments on the behavior of cracks in concrete subject to sustained shear loading" Heron V. 35, No.1, pp. 3 – 80.
22. Ata El-kareim Shoeib, (2005) “Efficiency of used glass fiber reinforced polymer for strengthening concrete and reinforced concrete elements of constructions,” Ph.D. thesis, Belgorod State Technological University, Belgorod, Russia, p. 159.
23. Bazant Z.P. and B.H. Oh, (1985) “Rock fracture via strain softening finite elements,” J. Eng. Mech. Asc V. 110, pp. 1015 – 1035.
24. Menetrey, P. and Willam, K.J., (1995) “Triaxial failure criterion for concrete and its generalization,” ACI Structural Journal, V. 93, No. 3, pp. 311-318.
25. Bazant Z.P. and B.H. Oh, (1983) “Crack band theory of fracture of concrete,” Mater struct [RILEM paris], pp. 155 – 177.
26. Cole, C. and Belarbi, A., (2001) “Confinement Characteristics of Rectangular FRP-Jacketed RC Columns” Proceedings of the Fifth International Symposium on Fiber Reinforced Polymer for Reinforced Concrete Structures (FRPRCS-5), Cambridge, UK, pp. 823-832.
27. Purba BK, Mufti AA., (1999) “Investigation of the behavior of circular concrete columns reinforced with carbon fiber reinforced polymer (CFRP) jackets,” Can J Civ. Eng., Vo. 26, pp. 590 – 596.

APPENDICES

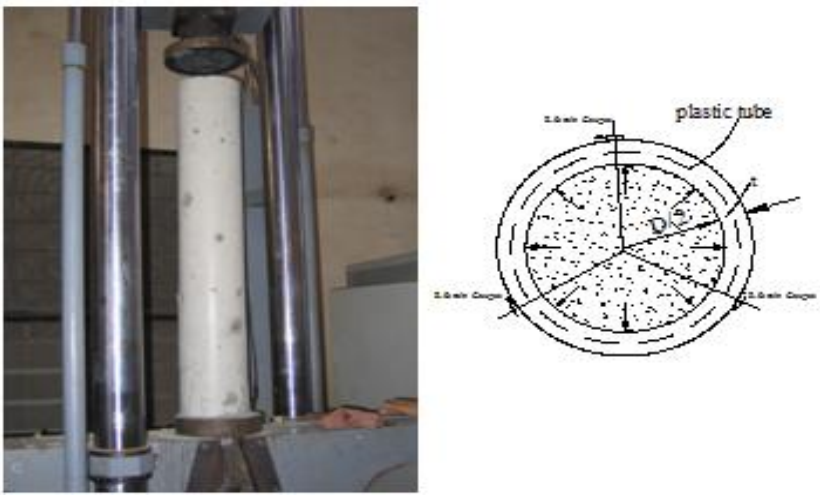

a) Universal Test Machine with Specimen b) Cross Section

Figure 1: Test Set up

a) [SUC6-40] b) [SUC5-60]

c) [SCC6-40] d) [SCC5-60]

Figure 2: The Mode of Failure for Confined and Unconfined Columns with Different Dimension

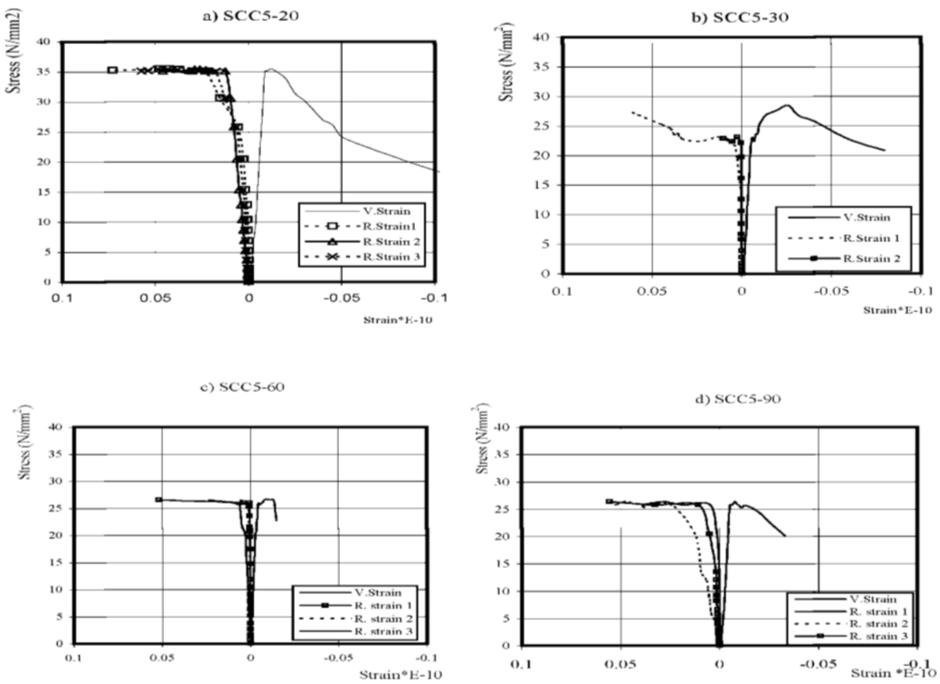

Figure 3: Stress-Strain Curves (Three Radial Strains and One Axial Strain) of Confined Concrete Column with Diameter 150mm and Different Heights

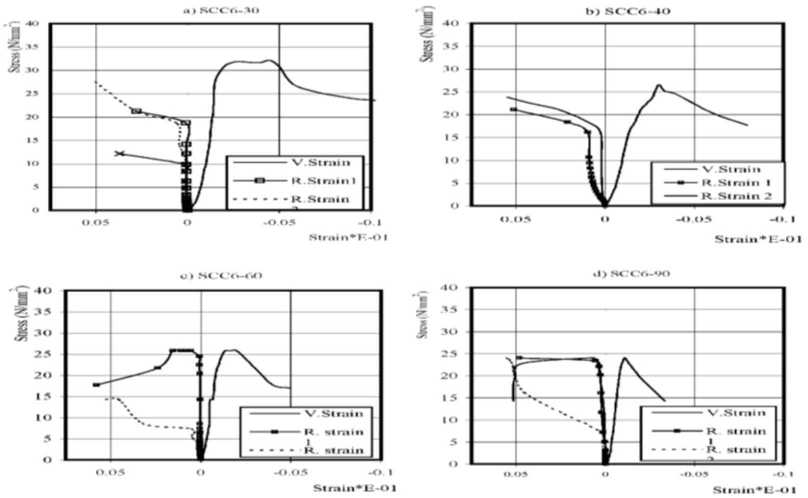

Figure 4: Stress-Strain Curves (Three Radial Strains and One Axial Strain) of Confined Concrete Column with Diameter 110mm and Different Heights

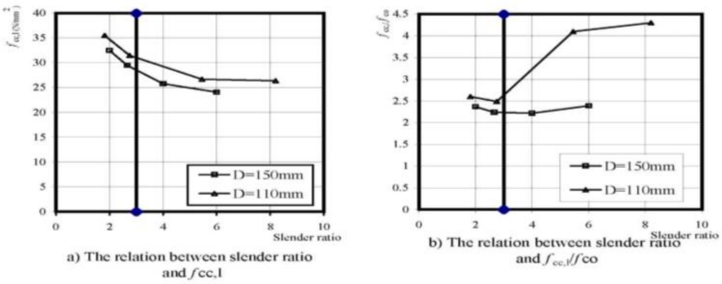

Figure 5: The effect of Slenderness Ratio on the Ultimate Stresses

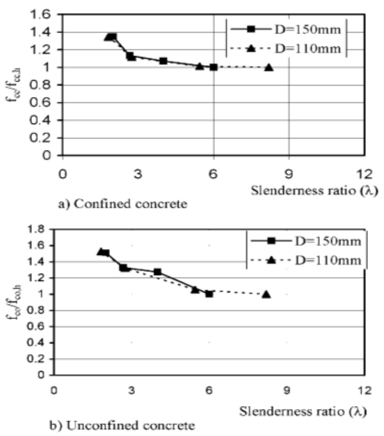

Figure 6: The Relation Between the Effect of the Slenderness Ratios $f_{co}/f_{co,h}$ and f_{cc},$f_{cc,h}$

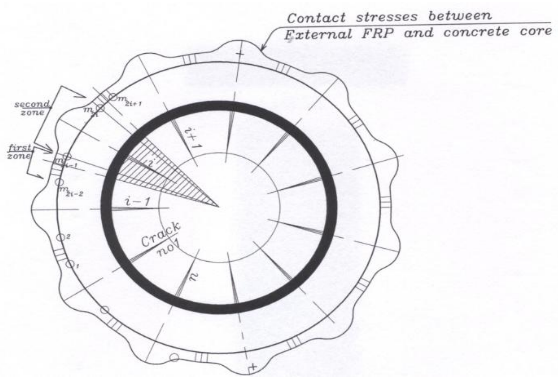

a. Proposal Cracks Distribution through Confined Concrete Core

b) Real Cracks Distribution through Confined Concrete Core [26]

Figure 7: Confined Cracks Model in Macro Scale

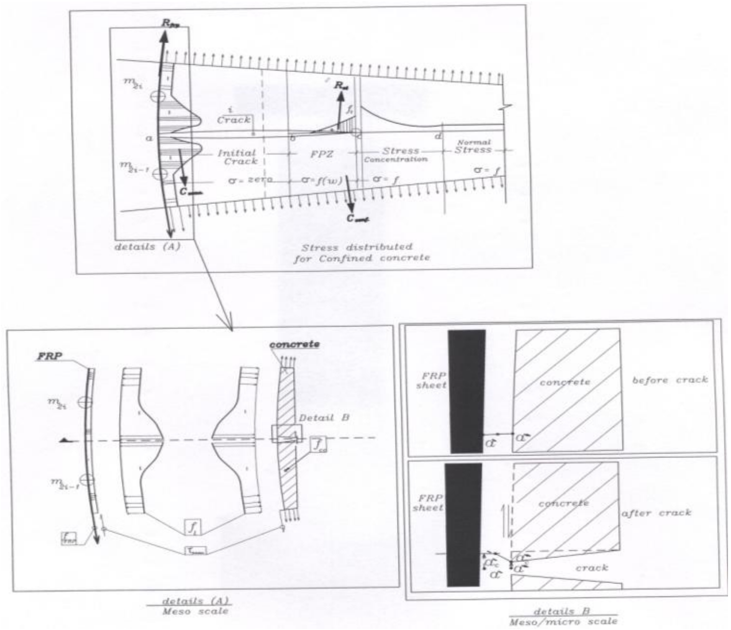

Figure 8: Stress Distribution, and Resistance and Acting Forces Position (Confined Concrete Model for Meso/Micro Scale)

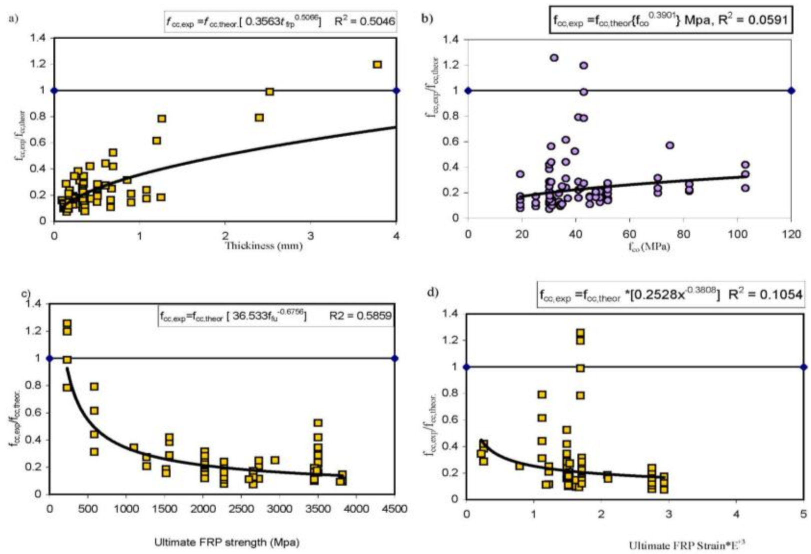

Figure 9: Evaluation the Theoretical Model According to Effect of a) Change Fiber Thickness b) Change Compressive Strength c) Ultimate Fiber Strength d) Ultimate Fiber Strain [25]

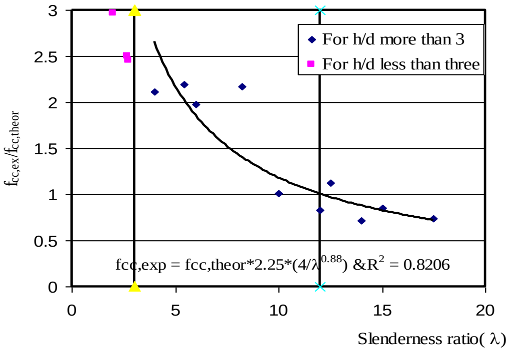

Figure 10: The Relation Between $f_{cc,exp}/f_{cc,th}$ and Slenderness Ratio λ

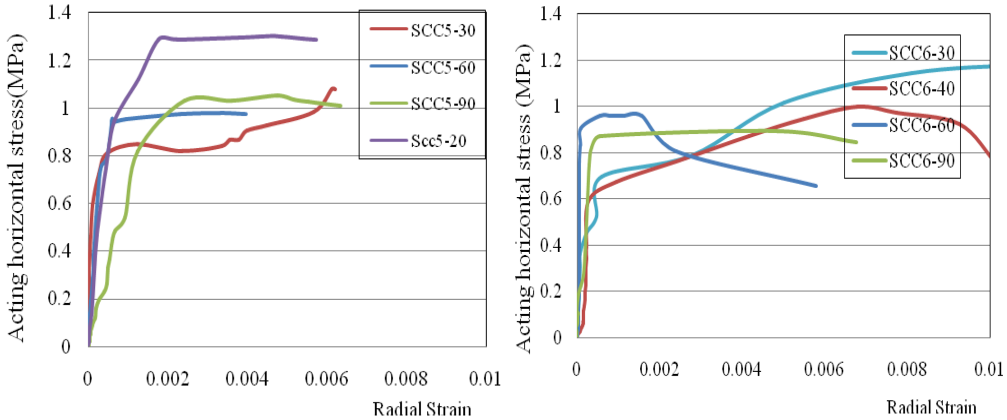

a) Group No. 1 **b) Group No. 2**

Figure 11: The Relation between Acting Horizontal Stress and Radial/Tangential Strain

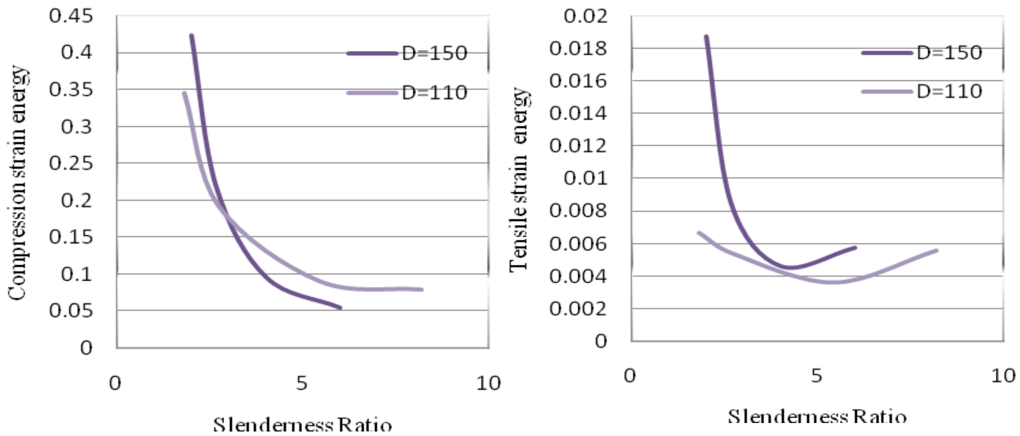

a) Compression Strain Energy (G_c) **b) Tensile Strain Energy (G_f)**

Figure 12: The Relation between Strain Energy and Slenderness Ratio

Table 1: Variation of Parameters Studies for Researchers

Author	Variation in Experiment Tested Specimens
Ahmed and et al 1991	Using GFRP, fco =39MPa, 50MPa, and 65MPa
Nanni and Bradford 1995	Used GFRP with thickness = 0.30mm, 0.60mm, 1.20mm
Harmon and et. al. 1992	Used GFRP with thickness = 0.089mm, 0.179mm, 0.344mm and 0.689mm and fco =41MPa and 103MPa
Picher and et. al. 1996	Used CFRP
watanabe et. al. 1997	Used CFRP and AFRP with thickness from 0.14mm to 0.435mm
Miyauchi et. al. 1997	Used CFRP with thickness=0.11mm and 0.22mm and variation

Table 1: Contd.,

Kono and et. al.(1998)	mm and 0.334 ,mm0.167=essUsed CFRP with thickn mm0.501
Toutanji and et. al (1999)	Comparing between CFRP and AFRP with thickness variations
Matthys and et. al. (1999)	Used CFRP with thickness 0.17mm, and 0.235mm
Shahawy and et. al.(2000)	Used CFRP with thickness variation and fco =19.4MPa and 49.0MPa
Rochette and Labossiere, 2000	Comparing between CFRP and AFRP with thickness variations
Micelli and et. al. (2001)	Comparing between GFRP and CFRP
Rousakis. (2001)	Used CFRP with variations fco from 25.15MPa to 82.13MPa
Mirmiran and shahawy 1997	Used GFRP tube with thickness=1.44mm, 2.2mm, and 2.97mm

Table 2: Comparing between Theoretical Models

Model	Theoretical f_{cc}
Saadatm et al.	$\frac{f_{cc}}{f_{co}} = 2.254\sqrt{1+7.94\frac{f_l}{f_{co}}} - \frac{2f_l}{f_{co}} - 1.254$
Miyauchie et al	$\frac{f_{cc}}{f_{co}} = 1 + 3.485 \times \frac{f_l}{f_{co}}$
Kono et al	$\frac{f_{cc}}{f_{co}} = 1 + 0.0572 \times f_l$
Saamen et al.	$\frac{f_{cc}}{f_{co}} = 1 + 6.0 \times \left(\frac{f_l}{f_{co}}\right)^{0.7}$
Toutanji	$\frac{f_{cc}}{f_{co}} = 1 + 3.5 \times \left(\frac{f_l}{f_{co}}\right)^{0.85}$
Xiao and Wu	$\frac{f_{cc}}{f_{co}} = 1.10 + \left[4.1 - 0.75\frac{E^2}{f_f}\right] \times \left(\frac{f_l}{f_{co}}\right)$

Table 3: Test Parameters

	Test Specimens	T(mm)	D(mm)	H.(mm)	H/D	D/2t
G1	SCC6-30	4.7	150	300	2	16.02
	SCC6-40	4.7	150	400	2.66	16.02
	SCC6-60	4.7	150	600	4.00	16.02
	SCC6-90	4.7	150	900	6.0	16.02
G2	SCC5-20	3.7	110.0	200	1.82	15.62
	SCC5-30	3.7	110.0	300	2.75	15.62
	SCC5-60	3.7	110.0	600	5.45	15.62
	SCC5-90	3.7	110.0	900	8.2	15.62

Table 4: Test Parameters and Results for Unconfined Concrete Column

Group	Test Specimens	D (mm)	H (mm)	H/D	f_{co} N/mm^2
G3	SUC6-30	150.0	300	2	13.75
	SUC6-40	150.0	400	2.66	12.30
	SUC6-60	150.0	600	4.00	11.6
	SUC6-90	150.0	900	6.0	10.1
G4	SUC5-20	110.0	200	1.82	13.75
	SUC5-30	110.0	300	2.75	11.9
	SUC5-60	110.0	600	5.45	6.5
	SUC5-90	110.0	900	8.2	6.0

Table 5: Material Properties of the Concrete

f_{cu} (MPa) (150x300mm)	f_{cu} (MPa) (150×150×150mm).	E_c (GPa) (150x300 mm)
13.75	16.5	19

Table 6: Experimental Ultimate Stresses Results for Confined Concrete Columns with Plastic Tube

Group	Test Specimens	H/D	P_{max} Ton	f_{co} N/mm^2	f_{cc} N/mm^2	f_{cc}/f_{co}	$f_{co}/f_{co,h}$	$f_{cc}/f_{cc,h}$
G1	SCC6-30	2.00	47.50	13.75	32.50	2.37	1.51	1.35
	SCC6-40	2.67	40.00	12.10	27.30	2.24	1.33	1.33
	SCC6-60	4.00	38.00	11.60	25.80	2.22	1.28	1.07
	SCC6-90	6.00	37.00	9.10	24.10	2.39	1	1
G2	SCC5-20	1.82	29.30	13.75	35.50	2.60	1.53	1.35
	SCC5-30	2.75	23.50	11.9	29.50	2.49	1.42	1.18
	SCC5-60	5.45	22.75	9.5	26.70	4.10	1.06	1.01
	SCC5-90	8.2	21.80	9.0	26.40	4.3	1	1
f_{co}(h) and f_{cc} (h) is the unconfined and confined strength at 900mm heights								

Table 7: Calculted Compressive and Tensile Strain Energy

Group	Test Specimens	H/D	G_c Under (f_{cc}-ε_{ax}) curve MPa/(mm/mm)	G_f Under (f_{sp}-ε_{ra}) curve MPa/(mm/mm)	G_c/G_f
G1	SCC6-30	2.00	0.423	0.01874	22.57
	SCC6-40	2.67	0.2195	0.008558	25.65
	SCC6-60	4.00	0.0969	0.004655	20.82
	SCC6-90	6.00	0.0551	0.00578	9.53
G2	SCC5-20	1.82	0.354	0.0067	52.84
	SCC5-30	2.75	0.1918	0.00539	35.58
	SCC5-60	5.45	0.0907	0.00361	25.12
	SCC5-90	8.2	0.079	0.0056	14.11

Table 8: Comparing Between Proposal Model, Different Analytical Models

$f_{cc,\,experimental} / f_{cc,\,theoretical}$						$f_{cc,\,theoretical}$ (MPa)										
eq (25)	Toutanji	Saamen et al.	Kono et al	Miyauchie et al	Saadatm et al.	eq (22)	eq (25)	Toutanji	Saamen et al.	Kono et al	Miyauchie et al	Saadatm et al.	f_{cc} MPa	H/d	Test specimen	Group
1.18	1.78	1.28	2.25	1.95	1.19	12.19	27.43	18.26	25.49	14.42	16.71	27.23	32.5	2	SCC6-30	G3
1.00	1.03	1.03	1.89	1.60	0.94	12.19	27.43	26.58	26.58	14.42	17.11	29.07	27.3	2.66	SCC6-40	
0.80	0.96	0.96	1.79	1.50	0.87	12.19	32.40	26.97	26.97	14.42	17.25	29.73	25.8	4	SCC6-60	
1.06	0.82	0.82	1.67	1.32	0.71	12.19	22.68	29.42	29.42	14.42	18.22	34.12	24.1	6	SCC6-90	
1.29	1.25	1.25	2.42	2.00	1.10	12.43	27.44	28.33	28.33	14.66	17.78	32.13	35.5	1.82	SCC5-20	G4
1.08	0.99	0.99	2.01	1.60	0.84	12.43	27.44	29.88	29.88	14.66	18.41	34.99	29.5	2.75	SCC5-30	
1.08	0.82	0.82	1.82	1.36	0.66	12.43	24.68	32.64	32.64	14.66	19.58	40.36	26.7	5.45	SCC5-60	
1.53	0.79	0.79	1.80	1.33	0.63	12.43	17.23	33.37	33.37	14.66	19.91	41.83	26.4	8.2	SCC5-90	
0.82	0.28	0.28	0.62	0.46	0.22	12.19	10.96	32.58	32.58	14.42	19.56	40.23	8.96	14	CG11	**G1***
0.82	0.32	0.32	0.72	0.53	0.26	12.19	12.56	32.58	32.58	14.42	19.56	40.23	10.35	12	CG12	
0.85	0.39	0.39	0.87	0.64	0.31	12.19	14.74	32.58	32.58	14.42	19.56	40.23	12.59	10	CG13	
1.02	0.25	0.25	0.62	0.42	0.18	12.43	9.01	37.14	37.14	14.66	21.67	49.86	9.15	17.5	CG21	**G2***
1.03	0.29	0.29	0.73	0.49	0.21	12.43	10.32	37.14	37.14	14.66	21.67	49.86	10.63	15	CG22	
1.15	0.38	0.38	0.95	0.64	0.28	12.43	12.12	37.14	37.14	14.66	21.67	49.86	13.95	12.5	CG23	

G1*, G2* is the long confined concrete model